Published in final edited form as:
Circ Res. 2012 August 17; 111(5): e111–e122. doi:10.1161/CIRCRESAHA.112.265587.

Functional Redundancy of SWI/SNF Catalytic Subunits in Maintaining Vascular Endothelial Cells in the Adult Heart

Monte S. Willis, M.D., Ph.D.[1,2], **Jonathon W. Homeister, M.D., Ph.D.**[1,2], **Gary B. Rosson, Ph.D.**[3], **Yunus Annayev, B.S.**[3], **Darcy Holley, B.S., B.S.**[3], **Stephen P. Holly, Ph.D.**[4], **Victoria J. Madden, B.S.**[1], **Virginia Godfrey, D.V.M., Ph.D.**[1], **Leslie V. Parise, Ph.D.**[2,4,5], and **Scott J. Bultman, Ph.D.**[3,5]

[1]Department of Pathology and Laboratory Medicine, University of North Carolina, Chapel Hill, NC 27599, USA

[2]McAllister Heart Institute, University of North Carolina, Chapel Hill, NC 27599, USA

[3]Department of Genetics, University of North Carolina, Chapel Hill, NC 27599, USA

[4]Department of Biochemistry and Biophysics, University of North Carolina, Chapel Hill, NC 27599, USA

[5]Lineberger Cancer Center, and University of North Carolina, Chapel Hill, NC 27599, USA

Abstract

Rationale—SWI/SNF chromatin-remodeling complexes utilize either BRG1 or BRM as a catalytic subunit to alter nucleosome position and regulate gene expression. BRG1 is required for vascular endothelial cell (VEC) development and embryonic survival, whereas BRM is dispensable.

Objective—To circumvent embryonic lethality and study *Brg1* function in adult tissues, we utilized conditional gene targeting. To evaluate possible *Brg1-Brm* redundancy, we analyzed *Brg1* mutant mice on wild-type and *Brm*-deficient backgrounds.

Methods and Results—The inducible *Mx1-Cre* driver was used to mutate *Brg1* in adult mice. These conditional-null mutants exhibited a tissue-specific phenotype and unanticipated functional compensation between *Brg1* and *Brm. Brg1* single mutants were healthy and had a normal lifespan, whereas *Brg1/Brm* double mutants exhibited cardiovascular defects and died within one month. BRG1 and BRM were required for the viability of VECs but not other cell types where both genes were also knocked out. The VEC phenotype was most evident in the heart, particularly in the microvasculature of the outer myocardium, and was recapitulated in primary cells *ex vivo*. VEC death resulted in vascular leakage, cardiac hemorrhage, secondary death of cardiomyocytes due to ischemia, and ventricular dissections.

Conclusions—BRG1-catalyzed SWI/SNF complexes are particularly important in cardiovascular tissues. However, in contrast to embryonic development, where *Brm* does not compensate, *Brg1* is required in adult VECs only when *Brm* is also mutated. These results demonstrate for the first time that *Brm* functionally compensates for *Brg1 in vivo* and that there are significant changes in the relative importance of BRG1- and BRM-catalyzed SWI/SNF complexes during the development of an essential cell lineage.

Correspondence to Scott J. Bultman, 120 Mason Farm Rd, Genetic Medicine Building, Room 5060, Chapel Hill, NC 27516-7264, Scott_Bultman@med.unc.edu, ph 919-966-3359; fax 919-843-4682.

Disclosures
None.

Keywords

BRG1; BRM; SWI/SNF; cardiac vascular endothelial cell; ventricular dissection

Introduction

The *Saccharomyces cerevisiae* SWI/SNF (mating type switching/sucrose non-fermenting) complex was the first chromatin-remodeling complex to be characterized and consists of 11 subunits with a total molecular mass of [1-2] MDa.1,2 SWI/SNF complexes have been evolutionarily conserved although mammals have approximately 21 subunits due to duplication and divergence events that occurred during vertebrate evolution.[3] Rather than having a larger-sized complex consisting of 21 subunits, mammals have a number of 9-12 subunit complexes with different combinatorial assemblies (up to n=288 in theory).[3,4] Subunit composition can change within a cell lineage as it differentiates and is known to vary among different tissues.[4,5] However, despite this subunit diversity, all mammalian SWI/SNF complexes identified thus far contain either BRG1 or BRM (brahma-related gene 1 and brahma, also known as SMARCA4 and SMARCA2, respectively) as a catalytic subunit with DNA-dependent ATPase activity.[3,4] Each complex also contains several core subunits (also known as BRG1/BRM-associated factors or BAFs) including BAF170, BAF155, and BAF47 (also known as SNF5 or SMARCB1).[3,4]

SWI/SNF-related complexes are recruited by sequence-specific transcription factors to the promoters of numerous target genes[6-8], where they slide or evict histone octamers in an ATP-dependent manner.[9,10] This alters the number and position of nucleosomes near transcriptional start sites (TSS) to regulate RNA Polymerase II occupancy and transcriptional initiation.[10-12] The importance of SWI/SNF complexes in mammalian development has been demonstrated by mouse knockout studies. Null mutations of *Brg1, Baf250a/Arid1a, Baf155*, and *Baf47/Snf5* each confer peri-implantation lethality. [4,13] This phenotype is consistent with the OCT4, SOX2, and Nanog pluripotency transcription factors recruiting a specific SWI/SNF subcomplex, called esBAF, to target genes in embryonic stem (ES) cells to facilitate their self-renewal and pluripotency. [7,14-16] Null mutations of the *Baf180* and *Baf60c* non-core subunits each result in mid-gestation lethality due to cardiac defects. [17,18] *Baf250a/Arid1a* null heterozygotes and *Brg1* conditional mutants also exhibit cardiovascular defects that are lethal at midgestation. [19-21]. At a mechanistic level, *Brg1* genetically interacts with *Tbx5*[21], and the BAF60c subunit facilitates a physical interaction between BRG1 and the cardiogenic transcription factors TBX5, GATA4, and Nkx2-5.[17] Furthermore, a combination of BAF60c plus TBX5 and GATA4 can program non-cardiac mesoderm into cardiomyocytes.[22,23] Based on these studies, SWI/SNF complexes have emerged as key epigenetic regulators of cardiomyocyte development.[22]

Cardiomyocyte development is coordinated with vascular development, and *Brg1* is also required for vasculogenesis based on the mid-gestation lethality of $Brg1^{Tie2\text{-}Cre}$ conditional mutants where *Brg1* was mutated in vascular endothelial cells (VECs) during embryogenesis.[24-26] The $Brg1^{Tie2\text{-}Cre}$ mutant phenotype was not exacerbated by *Brm* deficiency[25], which is surprising because Brm is expressed at high levels in the developing vasculature and encodes a protein that is 75% identical to BRG1 with similar or identical chromatin-remodeling properties on nucleosome arrays in cell-free systems.[27,28] This finding suggests that VECs may rely on the PBAF class of complexes, which utilize only BRG1 as their catalytic subunit, rather than the BAF class that utilizes either BRG1 or BRM.[3] This possibility has a precedent as the esBAF subcomplex utilizes BRG1 exclusively as a catalytic subunit. [7,14] Alternatively, BRG1 vascular function may occur in the context of BAF complexes, but BRM cannot compensate either because it interacts with different

transcription factors and is recruited to different target genes or it has different biochemical properties than BRG1 *in vivo*.[8] Support for this possibility comes from the observation that the two catalytic subunits have antagonistic roles in the differentiation of certain cell lineages.[29] Regardless of which possibility proves correct, BRG1 and BRM clearly have distinct functions. In fact, the function of BRM is different than all other SWI/SNF subunits that have been knocked out thus far because *Brm*$^{-/-}$ mice are viable and fertile instead of being embryonic lethal.[4,13,30]

Although BRG1-catalyzed SWI/SNF complexes are essential for cardiovascular development and other aspects of embryogenesis[4,13], it is not known whether they maintain cellular homeostasis after development is complete. To address this important issue, it was necessary to circumvent the requirement for *Brg1* during embryogenesis so we used the inducible *Mx1-Cre* driver to mutate *Brg1* in several tissues of adult *Brg1*$^{fl/fl}$ mice. By analyzing these conditional mutants on both wild-type and *Brm*-deficient backgrounds, we discovered an unprecedented genetic interaction between *Brg1* and *Brm* in cardiovascular homeostasis as described below.

Methods

An expanded Methods section is available in the Online Data Supplement at http://circres.ahajournals.org.

All mouse experiments were approved by the Institutional Animal Care and Use Committee (IACUC) review board at the University of North Carolina and were performed in accordance with federal guidelines. The *Brg1* floxed and Δfloxed alleles and the *Brm* mutation were genotyped by PCR as previously described.[30,31] To induce *Mx1-Cre in vivo*, mice were injected intraperitoneally with 300 mg of pI-pC (Sigma, St Louis, MO, USA) dissolved in PBS in a volume of 0.2 cc. Mice were injected every other day for a total of 5 treatments. Control mice received the same injection regimen but with PBS only.

Histology was performed by fixing heart and other tissues in 4% paraformaldehyde, embedding in paraffin, and cutting 5-μm sections according to standard procedures. Sections were either stained with H&E or processed for IHC using a BRG1 rabbit polyclonal antibody (Upstate/Millipore #07-478, Temecula, CA, USA) or a PECAM-1 antibody (Upstate/Millipore #04-1074, Temecula, CA, USA) according to the manufacturer's recommendations. X-Gal staining was performed using standard procedures on 200-μm vibratome slices of heart and other tissues from Rosa26 reporter (R26R, *Rosa-lox-stop-lox-LacZ*) mice carrying the *Mx1-Cre* transgene.

For electron microscopy, following perfusion with 2% paraformaldehyde and 2.5% glutaraldehyde in 0.15 M sodium phosphate buffer (pH 7.4), heart and other tissues were fixed in the same solution overnight and then post-fixed with 1% osmium tetroxide/0.15M sodium phosphate buffer. Samples were dehydrated with increasing concentrations of ethanol, infiltrated and embedded in Polybed 812 epoxy resin (Polysciences, Warrington, PA, USA), and 70-nm ultrathin sections were cut with a diamond knife. Sections were mounted on 200-mesh copper grids and staining with 4% aqueous uranyl acetate and Reynolds' lead citrate. Sections were observed with a LEO EM910 transmission electron microscope operating at 80 kV (LEO Electron Microscopy, Thornwood, NY, USA) and photographed with a Gatan-Orius SC1000 CCD Digital Camera and Digital Micrograph 3.11.0 (Gatan, Pleasanton, CA, USA).

Primary VECs were isolated and cultured as described with minor modifications.[32] Mouse hearts were minced and digested with collagenase solution [0.2 mg/mL type II collagenase (Worthington, Lakewood, NJ, USA) in Hank's Balanced Salt solution (Biowhittaker/Lonza,

Basel, Switzerland)] for 45 min at 37°C to generate single-cell suspensions. Cells were filtered through cell strainers and washed in base media (DMEM containing 25-mM HEPES, 20% FBS, 100U/100mg/mL penicillin-streptomyocin, and 2-mM glutamine). The samples were incubated with a biotinylated PECAM-1 antibody (BD Pharmingen, San Diego, CA, USA) for 10 min. Streptavidin-coated magnetic beads (Miltenyi Biotech, Auburn, CA, USA) were then added to the samples and incubated for 15 min at 4°C while rotating. The immunobead complex was then isolated by passing the samples through magnetic columns (Miltenyi Biotech), washing 3 times, and resuspending in complete culture media [basal media plus 100 mg/mL heparin (Sigma), 100 mg/mL endothelial cell growth stimulant (Biomedical Technologies, Stoughton, MA, USA), and sodium pyruvate (Invitrogen, Carlsbad, CA, USA)]. Cells were grown in 10-cm culture dishes pretreated with 0.1% gelatin in complete culture media under standard conditions (5% CO_2 at 37°C), and cultures were re-fed every other day and could be passaged several times while retaining their morphological appearance and PECAM-1-positive status. To induce Cre expression and mutate *Brg1*, pI-pC (Sigma) was added to VEC cultures at a final concentration of 100 μg/mL for 3 successive days.

Trans-thoracic echocardiography was performed on conscious mice using a VisualSonics Vevo 770 ultrasound biomicroscopy system (VisualSonics, Inc., Toronton, Ontario) with a 30-MHz 707B scan head as previously described.[33-35] Two-dimensional guided M-mode analysis of the left ventricle was performed in a genotype-blinded fashion in the plane of the parasternal long-axis at the level of the papillary muscle. Epi- and endo- cardium leading edges were used to the measure the anterior and posterior wall thickness (IVSTD, IVSTS), posterior wall thickness (PWTD, PWTS), and left ventricular internal diameters (LVEDD, LVESD). LV volume in diastole (LV VolD) was calculated from the equation LV VolD = (7/2.4 + LVEDD) × $LVEDD^3$ × 1000, and LV volume in systole (LV VolS) was calculated from the equation LV VolS = (7/2.4 + LVESD) × $LVESD^3$ × 1000. Left ventricular systolic function was assessed by ejection fraction (EF), calculated from the equation EF % = (LV VolD-LV VolS)/LV VolD × 100, and fractional shortening (FS), calculated from the equation FS % = (LVEDD-LVESD)/LVEDD × 100. M-mode measurements represent 3 average consecutive cardiac cycles from each mouse.

Results

Functional Compensation of *Brg1* and *Brm*

To investigate the role of *Brg1* in adult tissues, we crossed previously characterized *Mx1-Cre* transgenic mice and *Brg1* floxed mice to generate *Brg1* conditional null homozygotes ($Brg1^{fl/fl}$; $Mx1\text{-}Cre^{+/0}$). [31,36] Because *Mx1-Cre* is inducible, Cre is not expressed and the floxed-to-Δfloxed excision does not occur until after the mice have been injected with polyinosinic-polycytidylic acid (pI-pC), a synthetic double-stranded RNA that activates the interferon-responsive *Mx1* promoter.[36] Previous studies of *Mx1-Cre* using Rosa26 reporter (R26R) mice have demonstrated that pI-pC treatment results in Cre-mediated excision in the following cell types: hematopoietic stem cells and their descendants, hepatocytes, VECs throughout the body, the gastric epithelium, kidney (collecting ducts, glomeruli, and renal vascular endothelium), and smooth muscle in a subset of organs. [36,37] Therefore, each of these cell types will be functionally null in our *Brg1* conditional null homozygotes following pI-pC treatment. To assess excision of the *Brg1* locus, we performed PCR on tissues from $Brg1^{fl/fl}$; $Mx1\text{-}Cre^{+/0}$ mice. We detected the *Brg1* Δfloxed PCR product in mice that were treated with pI-pC but not in control mice that were treated with vehicle (PBS) or that were untreated (Figure 1A). These results confirmed that the *Brg1* excision event was induced by pI-pC as expected.

We administered either pI-pC or PBS to three categories of mice at 5-7 weeks of age and monitored their health and survival. The first category consisted of 40 control mice divided into four subcategories: 1, *Brg1*$^{fl/fl}$ mice lacking the *Mx1-Cre* transgene that were treated with pI-pC (n = 10); 2, *Brg1*$^{fl/fl}$ mice lacking the *Mx1-Cre* transgene on a *Brm*$^{-/-}$ background that were treated with pI-pC (n = 10); 3, *Brg1* conditional null homozygotes (*Brg1*$^{fl/fl}$; *Mx1-Cre*$^{+/0}$) that were treated with PBS (n = 10); 4, *Brg1* conditional null homozygotes on a *Brm*$^{-/-}$ background that were treated with PBS (n = 10). *Brg1* was not mutated in any of these control mice, and each animal was healthy and had normal survival as expected (Figure 1B). The second category was comprised of 25 single mutants: *Brg1* conditional null homozygotes on a wild-type (n = 15) or *Brm*$^{+/-}$ (n = 10) background that were treated with pI-pC (herein referred to as *Brg1*$^{Mx1\text{-}Cre}$ single mutants). All of these animals were also healthy and had normal survival (Figure 1B) and a normal lifespan (26 ± 5 months). The third category was double mutants: *Brg1* conditional null homozygotes on a *Brm*$^{-/-}$ background that were treated with pI-pC (n = 15). These mice (herein referred to as *Brg1*$^{Mx1\text{-}Cre}$/*Brm*$^{-/-}$ double mutants) either died or had to be euthanized within one month of pI-pC treatment due to their moribund condition (e.g. hunched posture, lethargy, labored breathing, and reduced response to direct contact) (Figure 1B). This phenotype was 100% penetrant as all 15 *Brg1*$^{Mx\text{-}Cre}$/*Brm*$^{-/-}$ double mutants became moribund. These results indicate that the *Brg1* and *Brm* catalytic subunits functionally compensate in the *Mx1-Cre* model.

Brg1$^{Mx1\text{-}Cre}$/*Brm*$^{-/-}$ Double-Mutant Mice Exhibit Cardiac Defects and Ventricular Dissections

To begin to understand the cause of death, *Brg1*$^{Mx1\text{-}Cre}$/*Brm*$^{-/-}$ double mutant mice were euthanized 20-30 days after pI-pC treatment, while they were moribund. Pleural effusions were present in nearly all mice, characteristically being a clear to blood-tinged fluid. Gross examination of these mice also revealed a kidney phenotype consistent with medullary congestion (Online Figure 1A). Other organ systems including the liver and gastrointestinal tract, were grossly unremarkable and indistinguishable from control mice.

Since pleural effusions can be associated with cardiac defects such as heart failure, we first analyzed the hearts and lungs from *Brg1*$^{Mx1\text{-}Cre}$/*Brm*$^{-/-}$ double mutants that had been treated 20-30 days earlier with pI-pC. Unlike control hearts (Figure 2A), numerous extravascular erythrocytes were identified within the myocardial interstitium of the atria and throughout the left and right ventricular myocardium from the apex to the base of double-mutant hearts (Figure 2B). This hemorrhage was particularly evident in the outer myocardium (representative sections shown in Figure 2B), while the endocardium and valve endothelium appeared normal at this level of magnification. Whereas the structural integrity of the aortic root, pulmonary artery, and coronary arteries remained intact (data not shown), we observed the subepicardial microvasculature as the primary source of the multifocal hemorrhages into the interstitium (Figure 2B). *Brg1*$^{Mx1\text{-}Cre}$/*Brm*$^{-/-}$ double-mutant hearts also exhibited areas of necrotic cardiomyocytes, a subset of which showed dystrophic calcification, scattered diffusely throughout the hemorrhagic myocardium (Figure 2B and Online Figure II), and this was associated with myocardial dissections identified by 2D echocardiography (Figure 2C). There were acute and chronic inflammatory cells within the affected myocardium, as well as reactive fibroblasts in areas with chronic cardiomyocyte injury (data not shown). Based on the analysis of Masson's Trichrome stained sections, *Brg1*$^{Mx1\text{-}Cre}$/*Brm*$^{-/-}$ double-mutant hearts also had significant fibrosis (Online Figure II) and cardiomyocyte hypertrophy (Online Figure IIIA). Quantification of cardiomyocyte cross-sectional areas revealed a 1.6-fold increase in double mutants compared to controls (Online Figure IIIB). In contrast to the heart, we did not detect any histopathologic abnormalities or abnormal cell death in the lungs or kidneys from *Brg1*$^{Mx1\text{-}Cre}$/*Brm*$^{-/-}$ double-mutant mice (Online Figure I).

To more carefully define the cardiac phenotype and provide insight into the kinetics of disease progression, we conducted a longitudinal echocardiographic study. Following pI-pC treatment, we performed daily trans-thoracic echocardiography on 9 conscious *Brg1*$^{Mx1\text{-}Cre}$/*Brm*$^{-/-}$ double mutants until each animal died or was euthanized due to humane endpoints. We also longitudinally analyzed 6 sibling-matched controls: 3 *Brg1*$^{Mx1\text{-}Cre}$/*Brm*$^{-/-}$ double mutants that were not treated with pI-pC, and 3 *Brg1*$^{fl/fl}$, *Brm*$^{-/-}$ mice lacking the *Mx1-Cre* transgene that were treated with pI-pC. On the first day of echocardiography (on the day after the final pI-pC treatment corresponding to day 9 in Figure 1B), we did not detect any significant differences for 15 quantitative measurements, referred to as “baseline”, between the treated double mutants and the two control groups (Figure 3A, Table 1). On subsequent echocardiographic studies, we detected an increased thickness of the anterior or posterior left ventricular wall of treated double mutants between 7 and 21 days later (median of 14 days) (Online Figure IV and Online Table I). In contrast, ventricular wall measurements did not change over time in any of the control mice (Online Figure IV). The left ventricular wall of the treated *Brg1*$^{Mx1\text{-}Cre}$/*Brm*$^{-/-}$ double mutant mice became progressively thicker over time (Online Figure IV). On the final echocardiogram, acquired one day before their death [(i.e., pre-mortem) median of 25 days following first echocardiogram (Online Table I) or 34 days following their first pI-pC treatment], the left ventricular wall of the *Brg1*$^{Mx1\text{-}Cre}$/*Brm*$^{-/-}$ double mutant mice was nearly twice that of controls (Figure 3A, Table 1). For example, the anterior wall thickness in diastole was 1.84 +/- 0.11 mm in treated double mutants compared to 1.04 +/- 0.04 mm and 1.06 +/- 0.02 mm in the two control groups (Figure 3A, Table 1). In addition to increased ventricular wall thickness, treated double mutants had a significant 2.4-fold increase in their left ventricular mass/body weight ratio and a 42% decrease in heart rate the day before their death (Figure 3A, Table 1).

In addition to the changes identified in wall thickness, a number of additional progressive cardiac defects were seen in the *Brg1*$^{Mx1\text{-}Cre}$/*Brm*$^{-/-}$ double mutants. We consistently observed pericardial and intracardiac fluid accumulation in both 2D and M-mode echocardiography (Figure 3B). The intracardiac fluid was associated with dissections of the anterior or posterior ventricular wall (Online Movies). We observed dissections in 56% of the treated double mutants, and they preceded death by 3-7 days with a median of 5 days (Online Table I). In addition, posterior wall stunning was identified in one treated *Brg1*$^{fl/fl}$, *Brm*$^{-/-}$ double mutant (Online Figure V and Online Movies).

Cardiac Vascular Endothelial Cell Death is the Primary Defect

To identify the primary cellular defect in the heart of *Brg1*$^{Mx1\text{-}Cre}$/*Brm*$^{-/-}$ double mutants, it was necessary to determine where BRG1 is normally expressed in the heart and where *Mx1-Cre* inactivates the floxed allele. Therefore, we performed immunohistochemistry (IHC) and discovered that BRG1 is normally expressed in both VECs and cardiomyocytes throughout the heart in a nuclear distribution (Figure 4A). Because *Mx1-Cre* activity has not been characterized in the heart, we crossed the *Mx1-Cre* transgene onto the R26R background and performed X-Gal staining on heart sections from these mice. Strong nuclear Cre activity was induced by pI-pC in VECs throughout the heart but not in the cardiomyocytes (Figure 4B). No Cre activity was detected in either cell type in control mice that either lacked the *Mx1-Cre* transgene or that were not treated with pI-pC as expected (Figure 4C). Therefore, although BRG1 is expressed in both VECs and cardiomyocytes within the heart, it is only mutated in VECs suggesting this is the primary cell type responsible for the cardiovascular phenotype in double mutants.

We first investigated cardiac vascular endothelial cells by IHC using PECAM-1 (platelet endothelial cell adhesion molecule, also known as CD31). A strong, continuous staining in vessels was identified in control mice (Figure 4D). In contrast, the cardiac vasculature of *Brg1*$^{Mx1\text{-}Cre}$/*Brm*$^{-/-}$ double mutants had a discontinuous staining in moribund mice at 20-30

days post-pI-pC administration (Figure 4E). This result suggested that a subset of endothelial cells within double-mutant hearts either no longer expressed PECAM-1, or were dead/absent. To distinguish between these possibilities, we performed transmission electron microscopy (TEM) at 25 days post pI-pC treatment. Two distinct phenotypes were seen in these cells. The first distinguishing phenotype of the pI-pC-treated double mutants was the presence of dying endothelial cells attached to live VECs in the capillaries (Figure 5A). Notably, the gap junctions were intact between the dying and live VECs (Figures 5A and B), as they were between live cells throughout the treated *Brg1*$^{Mx1\text{-}Cre}$/*Brm*$^{-/-}$ mutants and control mice. The second distinguishing feature of the pI-pC-treated double mutants is that they had variably thicker VECs with larger vesicles, compared to controls, including swollen mitochondria and rough endoplasmic reticulum (Figure 5C). Consistent with the histopathology seen in Figure 2, capillaries with breached endothelium were identified in areas of hemorrhage and clot (data not shown). Many of these microvascular remnants had immune cell infiltration, platelets, and proteinaceous material consistent with fibrin clot formation. As expected, there was a correlation between the presence of injured and necrotic cardiomyocytes and sites of hemorrhage.

Consistent with VECs being the primary cell type affected, it was the cell type where we first observed a cardiac phenotype in *Brg1*$^{Mx1\text{-}Cre}$/*Brm*$^{-/-}$ double mutants at earlier time-points following the induction of the *Brg1* mutation. For example, when we analyzed *Brg1*$^{Mx1\text{-}Cre}$/*Brm*$^{-/-}$ double mutants fourteen days after the first dose of pI-pC, while they still appeared healthy and before any hemorrhage could be detected in H&E-stained sections, the cardiomyocytes appeared normal, whereas the VECs were uniformly thickened with increased vacuolization (Figure 6B-6D) compared to VECs found in control mice (Figure 6A). At this 14-day post-pI-pC time point, however, we did not identify any endothelial cells that were necrotic or absent. This phenotype was consistent with the thickened endothelial cells seen at the later time point (days 20-30) shown in Figure 5A and 5B. Since we were unable to identify any necrotic or missing endothelial cells at day 14, but found them readily at days 20-30, this supports a model where mutation of *Brg1 and Brm* in the VEC is the primary event, which leads to VECs undergoing physical changes at or before day 14 and VEC cell death by day 25. The distinct cardiac phenotype appears to be a secondary consequence of this localized VEC death resulting in intramyocardial hemorrhage, ischemia, cardiomyocyte death, and cardiac dissection.

To evaluate VEC survival/lethality in more detail, we used PECAM-1 magnetic bead sorting to isolate and culture primary VECs from the hearts of conditional mutant and control mice. These primary VECs had a characteristic cobblestone appearance and were PECAM-1-positive *ex vivo*, and their identity was confirmed by RT-PCR since they were positive for the VEC markers VE-cadherin and FLK1/VEGFR2 (Online Figure VI). These same cells were negative for alpha smooth muscle actin and FLT4/VEGFR3, which are pericyte and lymphatic endothelial cell markers, respectively (Online Figure VI). Cultures were established from *Brg1*$^{fl/fl}$*; Mx1-Cre*$^{+/0}$ mice on a *Brm*$^{-/-}$ background and non-transgenic controls (*Brg1*$^{fl/fl}$ mice lacking the *Mx1-Cre* transgene on a *Brm*$^{-/-}$ background). However, none of the mice used in these experiments were treated with pI-pC so the VECs were functional for *Brg1* at the time of their derivation. Cells were then treated with pI-pC for 3 successive days, and cell number was monitored over a two-week period. Relative to day 0 (immediately prior to the first pI-pC treatment), the number of VECs from *Brg1*$^{fl/fl}$*; Mx1-Cre*$^{+/0}$*; Brm*$^{-/-}$ mice (double mutants) dropped to 70% at day 7 and then to 10% at day 14 (Figure 7A). In contrast, VECs from the same mice that were not treated with pI-pC *ex vivo* survived and proliferated increasing to 180% and 350% at days 7 and 14, respectively (Figure 7A). When a *BRG1* cDNA expression vector was introduced into these cells, it rescued the drop in cell number following pI-pC-induced deletion of the endogenous *Brg1* locus (Figure 7A). As a final control, the number of VECs from non-transgenic control mice

increased to a similar extent regardless of whether or not they were treated with pI-pC as expected (Figure 7A). These results demonstrate that the VEC phenotype is cell autonomous and occurs under normoxic conditions.

Following pI-pC treatment, the observed decrease in the number of double-mutant cells could be due to decreased cell proliferation and/or increased cell death. To distinguish between these possibilities, we performed BrdU incorporation, Annexin V, and propidium iodide assays. We did not observe a significant difference between double mutants and non-transgenic controls for BrdU incorporation (Figure 7B) but did observe a significant difference for Annexin V and PI staining (Figure 7B). These findings indicate that the drop in cell number *ex vivo* arises because of increased apoptosis and cell death rather than decreased cell proliferation, and this is consistent with the cell death observed *in vivo*. Also similar to the *in vivo* phenotype, the cell death that occurred *ex vivo* resulted in permeability defects based on permeability assays that measured the movement of FITC-dextran macromolecules through a monolayer of VECs cultured on transwell inserts. The barrier function of double-mutant cells was intact 1 day after pI-pC treatment but was compromised 7 days after pI-pC treatment (Figure 7C). To determine whether this phenotype is associated with a perturbation in canonical SWI/SNF function, we analyzed the expression of genes that are expressed in endothelial cells and are regulated by BRG1-catalyzed SWI/SNF-related complexes. Accordingly, RT-qPCR showed a significant decrease in the mRNA levels of *Cd44* and *Pitx2* in double-mutant cells. For this and the other assays, the phenotypes observed in $Brg1^{fl/fl}; Mx1\text{-}Cre^{+/0}; Brm^{-/-}$ primary VECs were dependent on pI-pC treatment as expected (Figure 7A-D).

Consequences of Vascular Permeability Defects

The occurrence of vascular permeability defects in $Brg1^{Mx1\text{-}Cre}/Brm^{-/-}$ mutants might be expected to result in increased platelet activation and clot formation. Indeed, ELISA assays demonstrated that plasma samples from $Brg1^{Mx1\text{-}Cre}/Brm^{-/-}$ mutant mice 30 days after their first pI-pC treatment had elevated levels of platelet activation factor (PAF) and thrombin compared to controls (Online Figure VIIA-B). Platelets isolated from the double-mutant mice were less reactive to collagen in aggregation assays (Online Figure VIID), which is consistent with a previous exposure to collagen as a result of compromised vessels. Platelets are consumed during the clotting process so thrombocytopenia might also be expected, and complete blood counts showed that $Brg1^{Mx1\text{-}Cre}/Brm^{-/-}$ mutant mice had lower numbers of platelets 30 days after the first pI-pC treatment compared to controls (Online Figure VIIE). Finally, one might also expect VEGF levels to be increased in an attempt to compensate for the loss of VECs, and ELISA assays demonstrated that this was the case (Online Figure VIIC). Taken together, these secondary effects are consistent with severe vascular permeability defects.

Discussion

Because SWI/SNF complexes are essential for embryonic development, we do not know whether they are required for cellular homeostasis in adults. To address this issue, we utilized the inducible *Mx1-Cre* driver to mutate the *Brg1* catalytic subunit in various tissues of adult mice. These conditional mutants exhibited extensive cell death in cardiac tissue but not in other cell types that were also mutated such as the hematopoietic lineages and hepatocytes. The tissue specificity of this cardiovascular phenotype is consistent with previous studies demonstrating that BRG1-catalyzed SWI/SNF complexes play a particularly important role in cardiovascular development *in utero*[17-21,24-26], but there is an important difference regarding redundancy. Previous studies have shown that BRM does not compensate for BRG1 in either cardiomyocytes or VECs during embryonic development[20,21,25], whereas our data clearly demonstrate that BRM does compensate in

VECs of adults. This difference suggests that only BRG1-catalyzed complexes function in the establishment of VEC lineages during embryogenesis, whereas both BRG1- and BRM-catalyzed complexes function in the maintenance of differentiated VECs in the adult.

The *Mx1-Cre* driver mutated *Brg1* in VECs within the heart but not in cardiomyocytes. Consequently, VEC death was the primary defect, which resulted in vascular leakage, hemorrhage, ischemia, and cardiomyocyte death as a secondary effect. The VEC phenotype was most evident in the microvasculature, which is relatively fragile because it lacks the structural support that larger vessels receive from surrounding smooth muscle and adventitia. Furthermore, the hemorrhages were almost entirely confined to the heart, somewhat favoring the epicardium more than the endocardium, despite the fact that the *Mx1-Cre* driver targets VECs throughout the body. This organ and regional specificity may be attributed to the cardiac microvasculature being exposed to the physical forces associated with heartbeat compared to other organs. In support of this idea, we observed ultramicroscopic changes in double-mutant tongues, which are also subjected to physical forces in rodents due to their licking and grooming behavior (Online Figure VIII). Notably, the double mutants had a marked increase in the number and size of veisculo-vacuolar organelles, which are associated with enhanced endothelial cell permeability (Online Figure VIII)[41]. We would expect to observe hemorrhages in other organs if the double mutants did not succumb to their cardiovascular defects and survived longer.

Vascular dissections have been studied most prominently in the aorta. When vascular dissections extend into the heart itself, there is a characteristic decrease in contractility, as seen in the present study. Recent studies have shown that an underlying cause of vascular dissections is the induction of apoptosis of smooth muscle cells in the aortic artery, which leads to the degradation of the media.[42] Recent clinical and basic research demonstrates that there is an inflammatory component to these dissections, which may initiate apoptosis.[43] The present study links endothelial cell death with cardiac dissections, which are generally extensions of aortic root dissections in humans. To our knowledge, *Brg1* and *Brm* are the first genes shown to protect against cardiac dissections. The cardiac VEC death observed *in vivo* was recapitulated in primary cells *ex vivo*. This finding demonstrates that VEC death due to loss of *Brg1/Brm* is cell autonomous and occurs under normoxic conditions (i.e., VEC death was not secondary to vascular leakage and ischemia).

In a previous study, we demonstrated that $Brg1^{+/-}$ mice developed mammary tumors, while $Brg1^{+/-}$, $Brm^{-/-}$ mice developed mammary and VEC (i.e., hemangiosarcoma) tumors.[44] This difference in tumor spectrum suggests that BRG1/BRM redundancy affects VEC homeostasis with respect to tumorigenesis in addition to cell viability. The finding that BRG1/BRM redundancy protects against oncogenic transformation instead of cell death in these mice is likely due to BRG1 dosage (+/- versus -/-) and the accumulation of mutations in other genes that protect against cell death. Because mutations of genes encoding SWI/SNF subunits are common in certain types of human primary tumors[45], it will be interesting to evaluate *BRG1* and *BRM* for point mutations when human hemangiosarcomas undergo deep sequencing.

Finally, a negative result from this study has important mechanistic implications. $Snf5^{Mx1\text{-}Cre}$ mutants exhibit a hematopoietic phenotype consistent with a hematopoietic stem cell (HSC) defect[46], but $Brg1^{Mx1\text{-}Cre}/Brm^{-/-}$ double mutants did not show this phenotype. Unlike the $Snf5^{Mx1\text{-}Cre}$ mutants, we observed normal hematopoietic cellularity within bone marrow in H&E-stained femur sections from $Brg1^{Mx1\text{-}Cre}/Brm^{-/-}$ double mutants (Online Figure IX). We also performed flow cytometry and observed normal numbers of hematopoietic stem cells, common myeloid progenitors, and common lymphoid progenitors (data not shown). This finding suggests that HSCs require SWI/SNF complexes

but in a non-canonical manner that is dependent on SNF5 but is independent of either catalytic subunit. It is surprising because SWI/SNF function is usually equated with the BRG1 or BRM DNA-dependent ATPase activity that remodels nucleosomes. Essentially all SNF5 co-purifies with SWI/SNF complexes, and it is not required for complex stability. [47,48] Furthermore, SNF5 protects against cancer in a BRG1-dependent manner[49,50], which suggests that the mechanism of SWI/SNF action is fundamentally different during early hematopoiesis. It is not clear how SNF5 and the other BAF subunits contribute to SWI/SNF function at the biochemical level in cancer or during development, but they probably do more than simply serve as scaffolding factors that stabilize complexes or enhance canonical catalytic activity as demonstrated previously.[28] These subunits are known to participate in the recruitment and DNA binding of complexes to downstream target genes, which is usually viewed in an ATPase-centric manner, but our results suggest that they also have crucial biochemical activities yet to be discovered. This idea is supported by a recent report of BAF250/ARID1 ubiquitination activity.[51]

Supplementary Material

Refer to Web version on PubMed Central for supplementary material.

Acknowledgments

We thank Janice Weaver (University of North Carolina Animal Histopathology Laboratory) for assistance in preparing histological specimens and Yuri Fedoriw, MD for his consultation on the hematological analysis of the bone marrow. Thanks also goes to the McAllister Heart Institute Mouse Cardiovascular Core Facility at UNC for the use of the ultrasound biomicroscopy system and the Microscopy Services Laboratory of the University of North Carolina for use of their electron microscope.

Sources of Funding

This work was supported by funding from the National Institutes of Health (CA125237 to SJB), the American Institute of Cancer Research (SJB), and The Prevent Cancer Foundation (SJB).

References

1. Winston F, Carlson M. Yeast SNF/SWI transcriptional activators and the SPT/SIN chromatin connection. Trends Genet. 1992; 8:387–391. [PubMed: 1332230]
2. Smith CL, Horowitz-Scherer R, Flanagan JF, Woodcock CL, Peterson CL. Structural analysis of the yeast SWI/SNF chromatin remodeling complex. Nat Struct Biol. 2003; 10:141–145. [PubMed: 12524530]
3. Wu JI, Lessard J, Crabtree GR. Understanding the words of chromatin regulation. Cell. 2009; 136:200–206. [PubMed: 19167321]
4. Ho L, Crabtree GR. Chromatin remodelling during development. Nature. 2010; 463:474–484. [PubMed: 20110991]
5. Lessard J, Wu JI, Ranish JA, Wan M, Winslow MM, Staahl BT, Wu H, Aebersold R, Graef IA, Crabtree GR. An essential switch in subunit composition of a chromatin remodeling complex during neural development. Neuron. 2007; 55:201–215. [PubMed: 17640523]
6. Euskirchen GM, Auerbach RK, Davidov E, Gianoulis TA, Zhong G, Rozowsky J, Bhardwaj N, Gerstein MB, Snyder M. Diverse roles and interactions of the SWI/SNF chromatin remodeling complex revealed using global approaches. PLoS Genet. 2011; 7:e1002008. [PubMed: 21408204]
7. Ho L, Jothi R, Ronan JL, Cui K, Zhao K, Crabtree GR. An embryonic stem cell chromatin remodeling complex, esBAF, is an essential component of the core pluripotency transcriptional network. Proc Natl Acad Sci U S A. 2009; 106:5187–5191. [PubMed: 19279218]
8. Kadam S, Emerson BM. Transcriptional specificity of human SWI/SNF BRG1 and BRM chromatin remodeling complexes. Mol Cell. 2003; 11:377–389. [PubMed: 12620226]

9. Dechassa ML, Sabri A, Pondugula S, Kassabov SR, Chatterjee N, Kladde MP, Bartholomew B. SWI/SNF has intrinsic nucleosome disassembly activity that is dependent on adjacent nucleosomes. Mol Cell. 2010; 38:590–602. [PubMed: 20513433]
10. Liu N, Balliano A, Hayes JJ. Mechanism(s) of SWI/SNF-induced nucleosome mobilization. Chembiochem. 2011; 12:196–204. [PubMed: 21243709]
11. Kim SI, Bultman SJ, Kiefer CM, Dean A, Bresnick EH. BRG1 requirement for long-range interaction of a locus control region with a downstream promoter. Proc Natl Acad Sci USA. 2009; 106:2259–2264. [PubMed: 19171905]
12. Kim SI, Bresnick EH, Bultman SJ. BRG1 directly regulates nucleosome structure and chromatin looping of the alpha globin locus to activate transcription. Nucleic Acids Res. 2009; 37:6019–6027. [PubMed: 19696073]
13. de la Serna IL, Ohkawa Y, Imbalzano AN. Chromatin remodelling in mammalian differentiation: Lessons from ATP-dependent remodellers. Nat Rev Genet. 2006; 7:461–473. [PubMed: 16708073]
14. Ho L, Ronan JL, Wu J, Staahl BT, Chen L, Kuo A, Lessard J, Nesvizhskii AI, Ranish J, Crabtree GR. An embryonic stem cell chromatin remodeling complex, esBAF, is essential for embryonic stem cell self-renewal and pluripotency. Proc Natl Acad Sci USA. 2009; 106:5181–5186. [PubMed: 19279220]
15. Kidder BL, Palmer S, Knott JG. SWI/SNF-BRG1 regulates self-renewal and occupies core pluripotency-related genes in embryonic stem cells. Stem Cells. 2009; 27:317–328. [PubMed: 19056910]
16. Singhal N, Graumann J, Wu G, Arauzo-Bravo MJ, Han DW, Greber B, Gentile L, Mann M, Scholer HR. Chromatin-remodeling components of the BAF complex facilitate reprogramming. Cell. 2010; 141:943–955. [PubMed: 20550931]
17. Lickert H, Takeuchi JK, Von Both I, Walls JR, McAuliffe F, Adamson SL, Henkelman RM, Wrana JL, Rossant J, Bruneau BG. Baf60c is essential for function of BAF chromatin remodelling complexes in heart development. Nature. 2004; 432:107–112. [PubMed: 15525990]
18. Wang Z, Zhai W, Richardson JA, Olson EN, Meneses JJ, Firpo MT, Kang C, Skarnes WC, Tjian R. Polybromo protein BAF180 functions in mammalian cardiac chamber maturation. Genes Dev. 2004; 18:3106–3116. [PubMed: 15601824]
19. Gao X, Tate P, Hu P, Tjian R, Skarnes WC, Wang Z. ES cell pluripotency and germ-layer formation require the SWI/SNF chromatin remodeling component BAF250a. Proc Natl Acad Sci U S A. 2008; 105:6656–6661. [PubMed: 18448678]
20. Hang CT, Yang J, Han P, Cheng HL, Shang C, Ashley E, Zhou B, Chang CP. Chromatin regulation by BRG1 underlies heart muscle development and disease. Nature. 2010; 466:62–67. [PubMed: 20596014]
21. Takeuchi JK, Lou X, Alexander JM, Sugizaki H, Delgado-Olguin P, Holloway AK, Mori AD, Wylie JN, Munson C, Zhu Y, Zhou YQ, Yeh RF, Henkelman RM, Harvey RP, Metzger D, Chambon P, Stainier DY, Pollard KS, Scott IC, Bruneau BG. Chromatin remodelling complex dosage modulates transcription factor function in heart development. Nat Commun. 2011; 2:187. [PubMed: 21304516]
22. Bruneau BG. Chromatin remodeling in heart development. Curr Opin Genet Dev. 2010; 20:505–511. [PubMed: 20702085]
23. Takeuchi JK, Bruneau BG. Directed transdifferentiation of mouse mesoderm to heart tissue by defined factors. Nature. 2009; 459:708–711. [PubMed: 19396158]
24. Griffin CT, Curtis CD, Davis RB, Muthukumar V, Magnuson T. The chromatin-remodeling enzyme BRG1 modulates vascular Wnt signaling at two levels. Proc Natl Acad Sci U S A. 2011; 108:2282–2287. [PubMed: 21262838]
25. Griffin CT, Brennan J, Magnuson T. The chromatin-remodeling enzyme BRG1 plays an essential role in primitive erythropoiesis and vascular development. Development. 2008; 135:493–500. [PubMed: 18094026]
26. Stankunas K, Hang CT, Tsun ZY, Chen H, Lee NV, Wu JI, Shang C, Bayle JH, Shou W, Iruela-Arispe ML, Chang CP. Endocardial BRG1 represses Adamts1 to maintain the microenvironment for myocardial morphogenesis. Dev Cell. 2008; 14:298–311. [PubMed: 18267097]

27. Dauvillier S, Ott MO, Renard JP, Legouy E. Brm (SNF2alpha) expression is concomitant to the onset of vasculogenesis in early mouse postimplantation development. Mech Dev. 2001; 101:221–225. [PubMed: 11231080]
28. Phelan ML, Sif S, Narlikar GJ, Kingston RE. Reconstitution of a core chromatin remodeling complex from SWI/SNF subunits. Mol Cell. 1999; 3:247–253. [PubMed: 10078207]
29. Flowers S, Nagl NG Jr, Beck GR Jr, Moran E. Antagonistic roles for BRM and BRG1 complexes in differentiation. J Biol Chem. 2009; 284:10067–10075. [PubMed: 19144648]
30. Reyes JC, Barra J, Muchardt C, Camus A, Babinet C, Yaniv M. Altered control of cellular proliferation in the absence of mammalian brahma (SNF2alpha). EMBO J. 1998; 17:6979–6991. [PubMed: 9843504]
31. Bultman S, Gebuhr T, Yee D, La Mantia C, Nicholson J, Gilliam A, Randazzo F, Metzger D, Chambon P, Crabtree G, Magnuson T. A BRG1 null mutation in the mouse reveals functional differences among mammalian SWI/SNF complexes. Mol Cell. 2000; 6:1287–1295. [PubMed: 11163203]
32. Lim YC, Luscinskas FW. Isolation and culture of murine heart and lung endothelial cells for in vitro model systems. Methods Mol Biol. 2006; 341:141–154. [PubMed: 16799196]
33. Duan J, Gherghe C, Liu D, Hamlett E, Srikantha L, Rodgers L, Regan JN, Rojas M, Willis M, Leask A, Majesky M, Deb A. Wnt1/beta-catenin injury response activates the epicardium and cardiac fibroblasts to promote cardiac repair. EMBO J. 2011; 31:429–442. [PubMed: 22085926]
34. Li HH, Willis MS, Lockyer P, Miller N, McDonough H, Glass DJ, Patterson C. Atrogin-1 inhibits AKT-dependent cardiac hypertrophy in mice via ubiquitin-dependent coactivation of forkhead proteins. J Clin Invest. 2007; 117:3211–3223. [PubMed: 17965779]
35. Willis MS, Ike C, Li L, Wang DZ, Glass DJ, Patterson C. Muscle ring finger 1, but not muscle ring finger 2, regulates cardiac hypertrophy in vivo. Circ Res. 2007; 100:456–459. [PubMed: 17272810]
36. Kuhn R, Schwenk F, Aguet M, Rajewsky K. Inducible gene targeting in mice. Science. 1995; 269:1427–1429. [PubMed: 7660125]
37. Schneider A, Zhang Y, Guan Y, Davis LS, Breyer MD. Differential, inducible gene targeting in renal epithelia, vascular endothelium, and viscera of Mx1cre mice. Am J Physiol Renal Physiol. 2003; 284:F411–417. [PubMed: 12529277]
38. Machida Y, Murai K, Miyake K, Iijima S. Expression of chromatin remodeling factors during neural differentiation. J Biochem. 2001; 129:43–49. [PubMed: 11134956]
39. Muchardt C, Bourachot B, Reyes JC, Yaniv M. Ras transformation is associated with decreased expression of the Brm/SNF2alpha ATPase from the mammalian SWI-SNF complex. EMBO J. 1998; 17:223–231. [PubMed: 9427756]
40. Reisman DN, Sciarrotta J, Bouldin TW, Weissman BE, Funkhouser WK. The expression of the SWI/SNF ATPase subunits BRG1 and BRM in normal human tissues. Appl Immunohistochem Mol Morphol. 2005; 13:66–74. [PubMed: 15722796]
41. Dvorak AM, Feng D. The vesiculo-vacuolar organeele (VVO): a new endothelial cell permeability organelle. J Histochemistry & Cytochemistry. 2001; 49:419–431.
42. Luo F, Zhou XL, Li JJ, Hui RT. Inflammatory response is associated with aortic dissection. Ageing Res Rev. 2009; 8:31–35. [PubMed: 18789403]
43. He R, Guo DC, Estrera AL, Safi HJ, Huynh TT, Yin Z, Cao SN, Lin J, Kurian T, Buja LM, Geng YJ, Milewicz DM. Characterization of the inflammatory and apoptotic cells in the aortas of patients with ascending thoracic aortic aneurysms and dissections. J Thorac Cardiovasc Surg. 2006; 131:671–678. [PubMed: 16515922]
44. Bultman SJ, Herschkowitz JI, Godfrey V, Gebuhr TC, Yaniv M, Perou CM, Magnuson T. Characterization of mammary tumors from Brg1 heterozygous mice. Oncogene. 2008; 27:460–468. [PubMed: 17637742]
45. Wilson BG, Roberts CW. SWI/SNF nucleosome remodellers and cancer. Nat Rev Cancer. 2011; 11:481–492. [PubMed: 21654818]
46. Roberts CW, Leroux MM, Fleming MD, Orkin SH. Highly penetrant, rapid tumorigenesis through conditional inversion of the tumor suppressor gene SNF5. Cancer Cell. 2002; 2:415–425. [PubMed: 12450796]

47. Wang W, Xue Y, Zhou S, Kuo A, Cairns BR, Crabtree GR. Diversity and specialization of mammalian SWI/SNF complexes. Genes Dev. 1996; 10:2117–2130. [PubMed: 8804307]
48. Doan DN, Veal TM, Yan Z, Wang W, Jones SN, Imbalzano AN. Loss of the Ini1 tumor suppressor does not impair the expression of multiple BRG1-dependent genes or the assembly of SWI/SNF enzymes. Oncogene. 2004; 23:3462–3473. [PubMed: 14990991]
49. Wang X, Sansam CG, Thom CS, Metzger D, Evans JA, Nguyen PT, Roberts CW. Oncogenesis caused by loss of the Snf5 tumor suppressor is dependent on activity of brg1, the ATPase of the SWI/SNF chromatin remodeling complex. Cancer Res. 2009; 69:8094–8101. [PubMed: 19789351]
50. Kia SK, Gorski MM, Giannakopoulos S, Verrijzer CP. SWI/SNF mediates polycomb eviction and epigenetic reprogramming of the Ink4b-Arf-Ink4a locus. Mol Cell Biol. 2008; 28:3457–3464. [PubMed: 18332116]
51. Li XS, Trojer P, Matsumura T, Treisman JE, Tanese N. Mammalian SWI/SNF-A subunit BAF250/ARID is an E3 ubiquitin ligase that targets histone H2B. Mol Cell Biol. 2010; 30:1673–1688. [PubMed: 20086098]

Non-standard Abbreviations and Acronyms

BRG1	brahma related gene 1
BRM	brahma
VEC	vascular endothelial cell
Mx1	myxovirus resistance gene 1
SWI/SNF	mating type switching/sucrose nonfermentation
BAF	BRG1/BRM-associated factor
pI-pC	polyinosine-polycytosine
IHC	immunohistochemstry
TEM	transmission electron microscopy
PECAM-1	platelet endothelial cell adhesion molecule 1
fl	floxed (flanked by loxP sites)
TSS	transcription start site
BW	body weight
LV	left ventricle
HR	heart rate
LVEDD	LV end diastolic dimension
LVESD	LV end systolic dimension
LV EF	ejection fraction percentage
LV Vol d	LV volume in diastole
LV Vol s	LV volume in systole
NO	nitric oxide

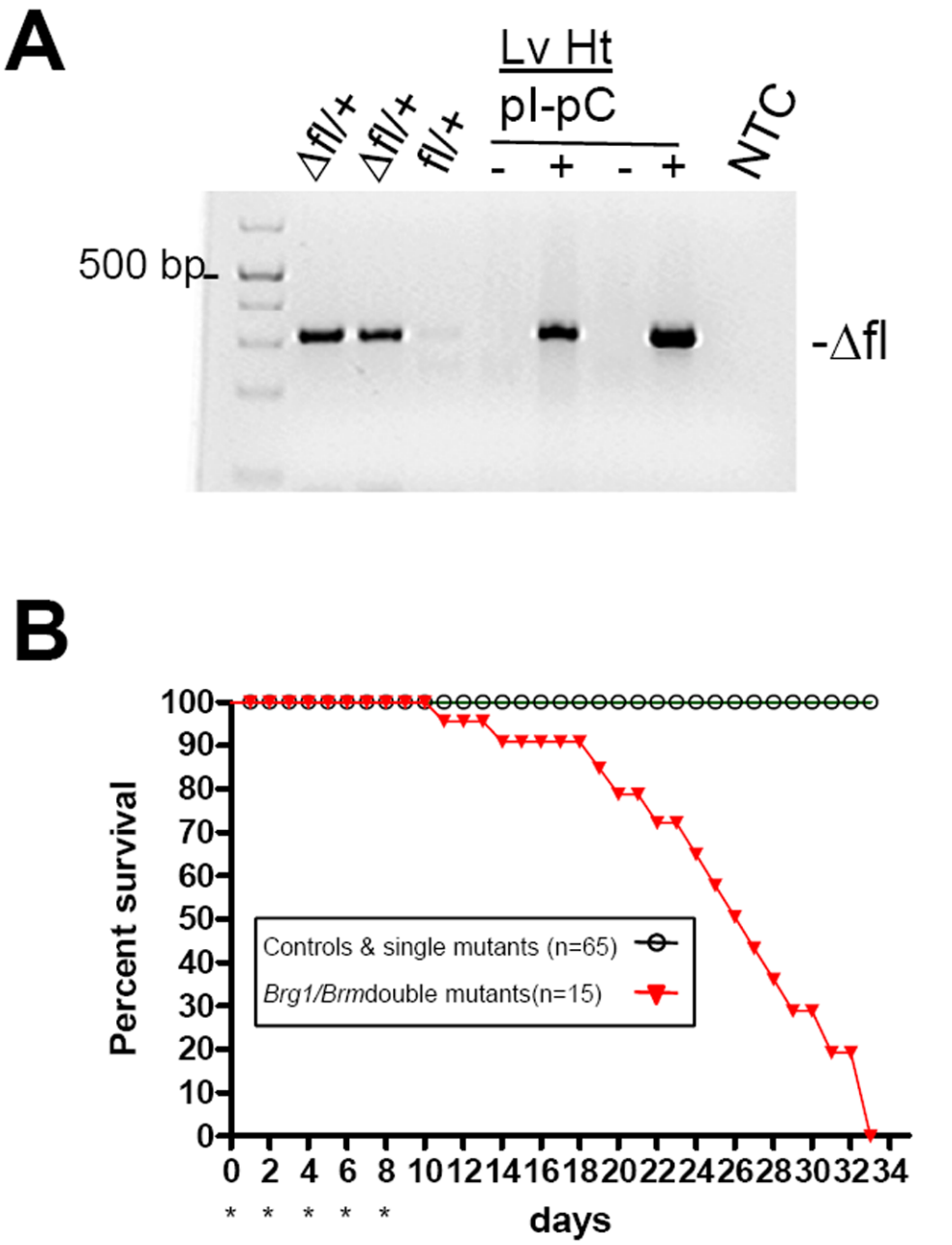

Figure 1. Rapid death of *Brg1/Brm* double mutants in the *Mx1-Cre* model following pI-pC treatment

A,Image of gel showing the *Brg1* Δfl PCR product from the following tissues. Lanes 1-3, tail tissue from control mice that were constitutively Δfl/+ (generated using a germline Cre driver) or fl/+; lanes 4-7, liver (Lv) and heart (Ht) tissue from untreated (-) and pI-pC treated (+) $Brg1^{fl/fl}$; $Mx1\text{-}Cre^{+/0}$ mice; lane 8, no template control (NTC). **B,** Kaplan-Meier survival curve of mice following administration of either pI-pC or PBS (denoted by asterisks on days 0, 2, 4, 6, and 8). Controls: $Brg1^{fl/fl}$ mice lacking the *Mx1-Cre* transgene that were treated with pI-pC (n = 10); $Brg1^{fl/fl}$ mice lacking the *Mx1-Cre* transgene on a $Brm^{-/-}$ background that were treated with pI-pC (n = 10); *Brg1* conditional null homozygotes ($Brg1^{fl/fl}$; $Mx1\text{-}Cre^{+/0}$) that were treated with PBS (n = 10); *Brg1* conditional null homozygotes on a $Brm^{-/-}$

background that were treated with PBS (n = 10). Single mutants: *Brg1* conditional null homozygotes on a wild-type (n = 15) or *Brm*$^{+/-}$ (n = 10) background that were treated with pI-pC. Double mutants: *Brg1* conditional null homozygotes on a *Brm*$^{-/-}$ background that were treated with pI-pC (n = 15).

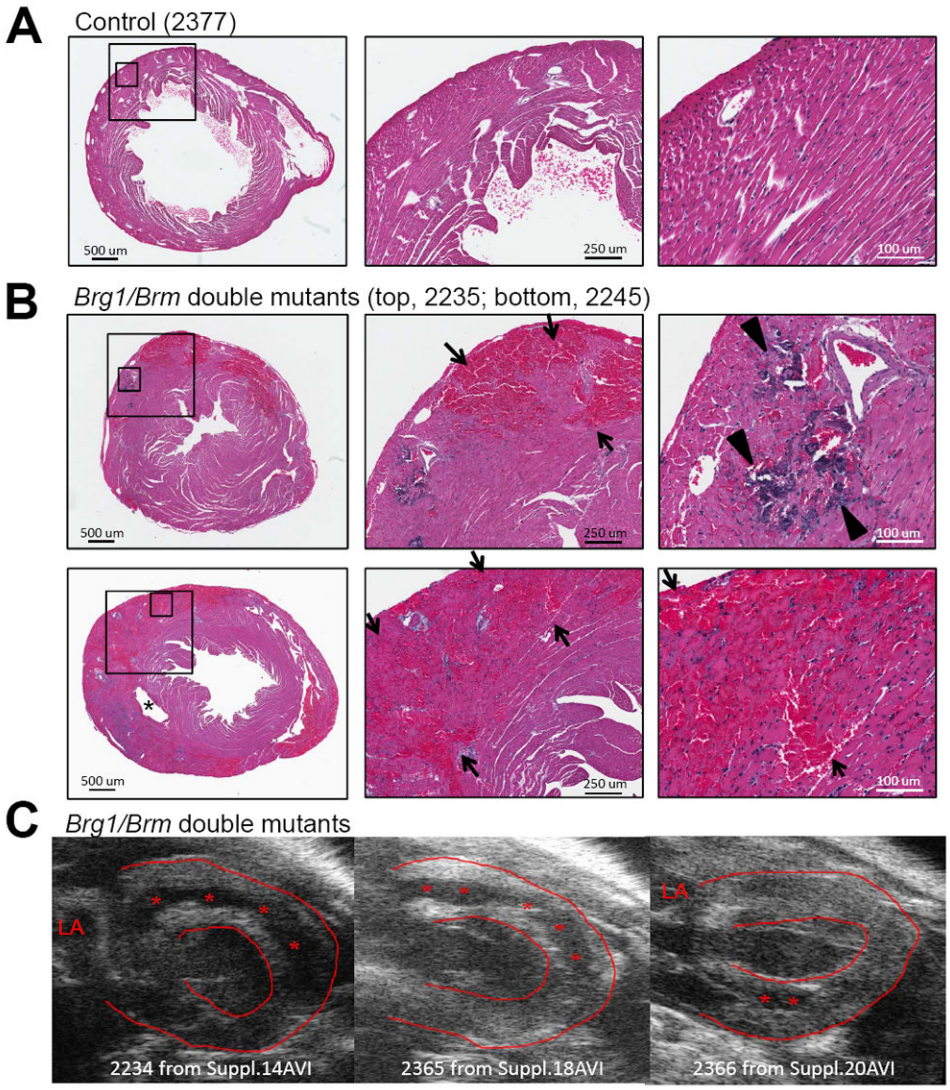

Figure 2. Histopathologic and 2D echocardiographic findings in *Brg1/Brm* double-mutant hearts

Representative images of H&E-stained heart sections from a control **(A)** and double-mutant **(B)** mice 25 days following pI-pC treatment. Animal numbers are indicated. The double-mutant hearts have diffuse and focal interstitial hemorrhage associated with myocyte necrosis (arrows) and calcification (arrow heads), particularly in the outer myocardium, which may result in myocardial dissection (panel C). *, artifactual disruption of ventricular wall due to fixative perfusion needle insertion. **(C)** Images extracted from 2D video outlining the anterior wall (top) and posterior wall (bottom) cardiac dissections identified after pI-pC treatment (see Online Table 1). The 2D video files are included (indicated in 2D image itself) in the supplemental data section. LA=left atria; *=area of dissection on day before death. 56% of mice had detectable dissections on mean day 38.8±9.9 (detailed in Online Table I).

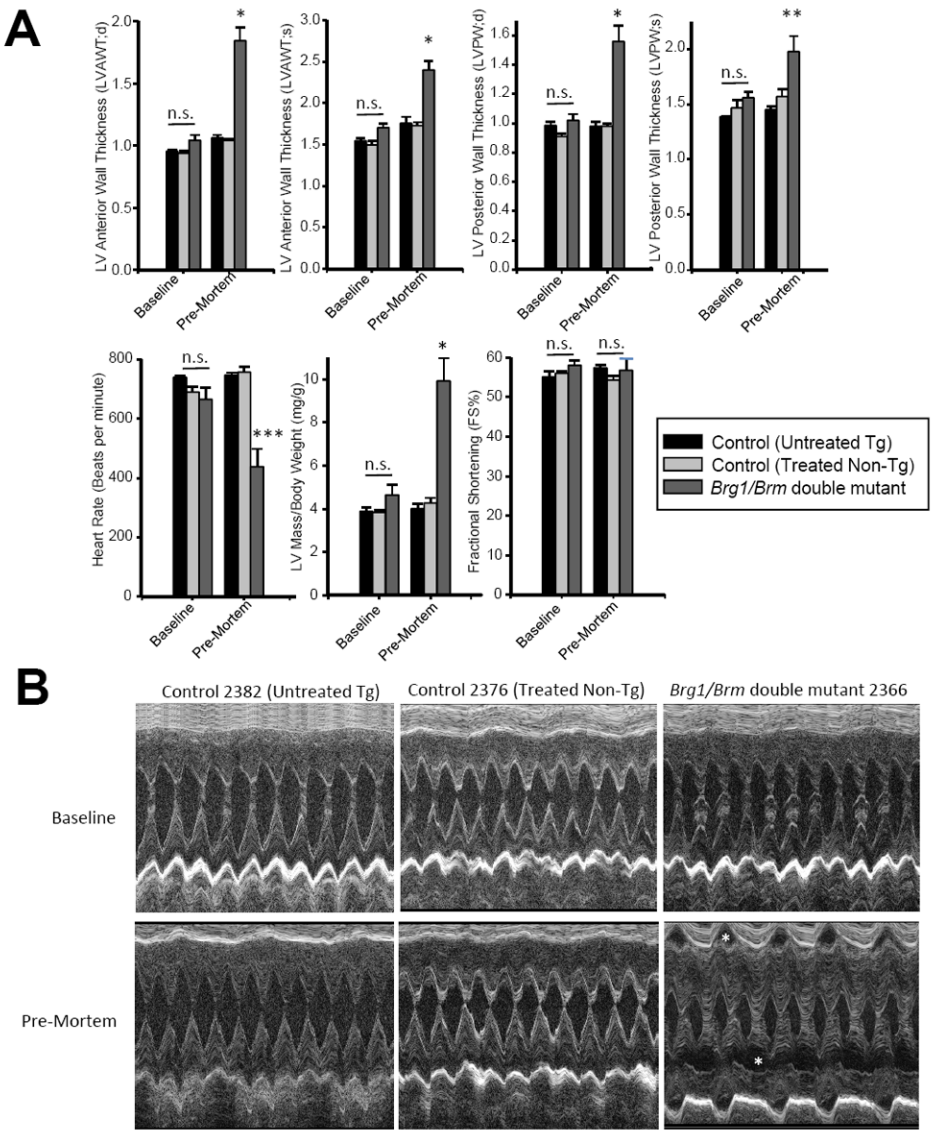

Figure 3. M-mode echocardiographic analysis of *Brg1/Brm* double-mutant mice

A,Quantitative measurements of controls and double mutants. Baseline values were taken one day after the final pI-pC treatment. Pre-mortem values were acquired one day before double mutants died or at an equivalent time point for controls. A one-way ANOVA was performed followed by a Holm-Sidak pair-wise comparison to determine significance between groups, *p<0.001, **p<0.03, ***p<0.01; n.s., not significant. **B,** M-mode cardiac phenotype of controls and double mutants at baseline and pre-mortem. The asterisks denote intracardiac fluid associated with ventricular dissection.

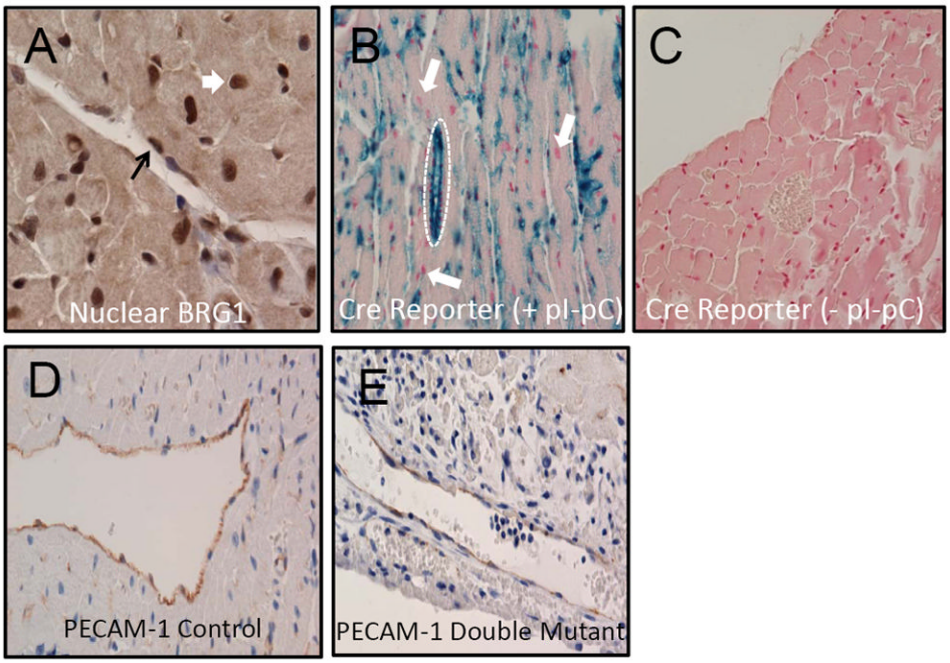

Figure 4. Expression analysis of BRG1, Mx1-Cre, and PECAM-1 in control and *Brg1/Brm* double-mutant cardiac VECs

(A) IHC demonstrating nuclear BRG1 staining in VECs (black arrow) and cardiomyocytes (white arrow) from a control mouse heart. **(B)** X-Gal staining of a representative heart section from pI-pC-treated R26R mice carrying the *Mx1-Cre* transgene. Strong staining (blue) occurred in VECs such as those enclosed by dashed circle, but staining was absent in cardiomyocytes as exemplified by the arrows. **(C)** No X-Gal staining occurred in heart sections from the same R26R mice carrying the *Mx1-Cre* transgene when they were not treated with pI-pC. **(D, E)** IHC demonstrating PECAM-1 staining of VECs in heart sections from control **(D)** and *Brg1/Brm* double-mutant **(E)** mice. A continuous staining of VECs was observed within control vessels **(D)**, whereas staining was discontinuous in double mutant vessels **(E)**.

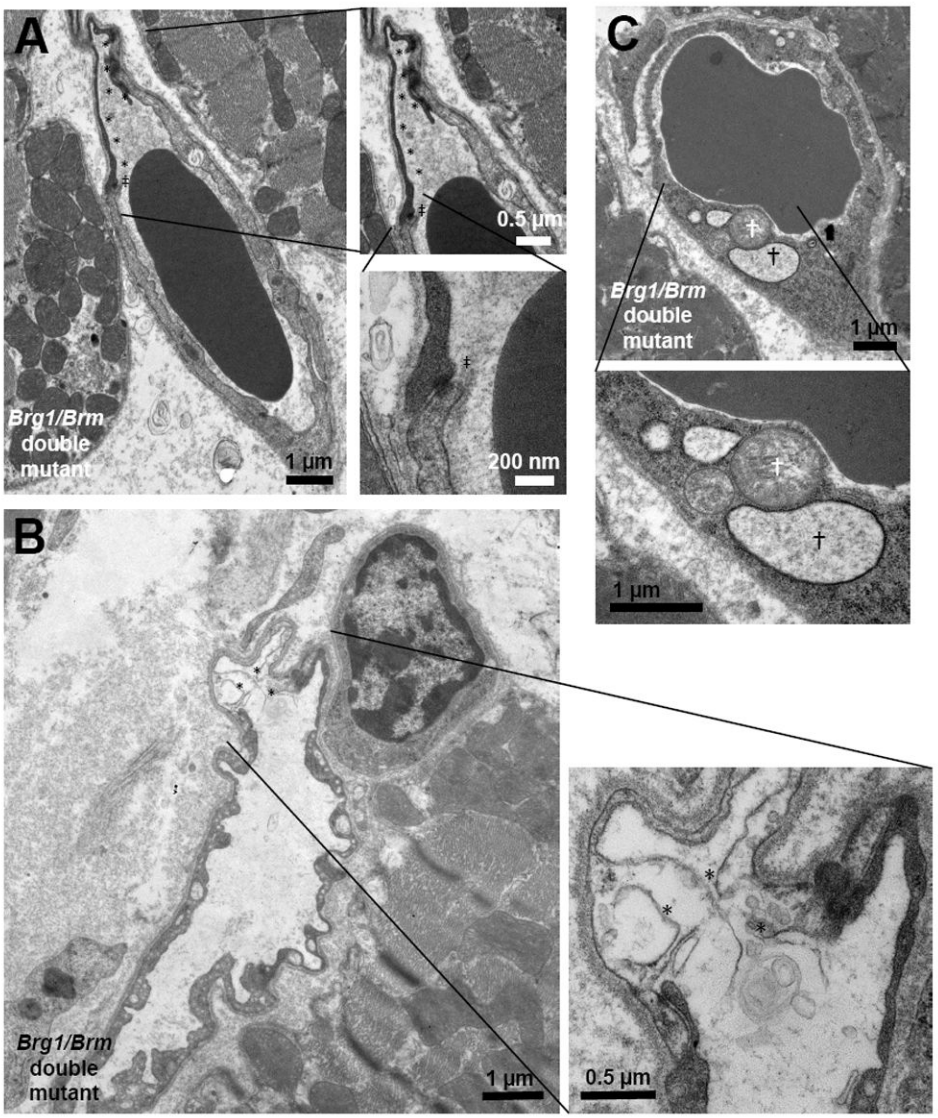

Figure 5. Ultrastructural defects in *Brg1/Brm* double mutants

Transmission electron microscopic analysis of cardiac endothelial cells demonstrates two general defects in many of the capillary vessel walls 25 days after the first pI-pC treatment in animal #2245. **(A & B)** Dying endothelial cells are present in the capillaries of treated *Brg1/Brm* double mutant mice (see *). Throughout the cardiac capillary bed, gap junctions between endothelial cells were intact between healthy cells as well as between affected cells. Note that even between viable and injured cells the gap junctions are intact (see ‡). **(C)** Vascular endothelial cells from treated *Brg1/Brm* double-mutant mice have swollen mitochondria (white †) and rough endoplasmic reticulum (black †), which are characteristic changes found in cell death. Panels A and C correspond to the epicardium, while panel B corresponds to the endocardium.

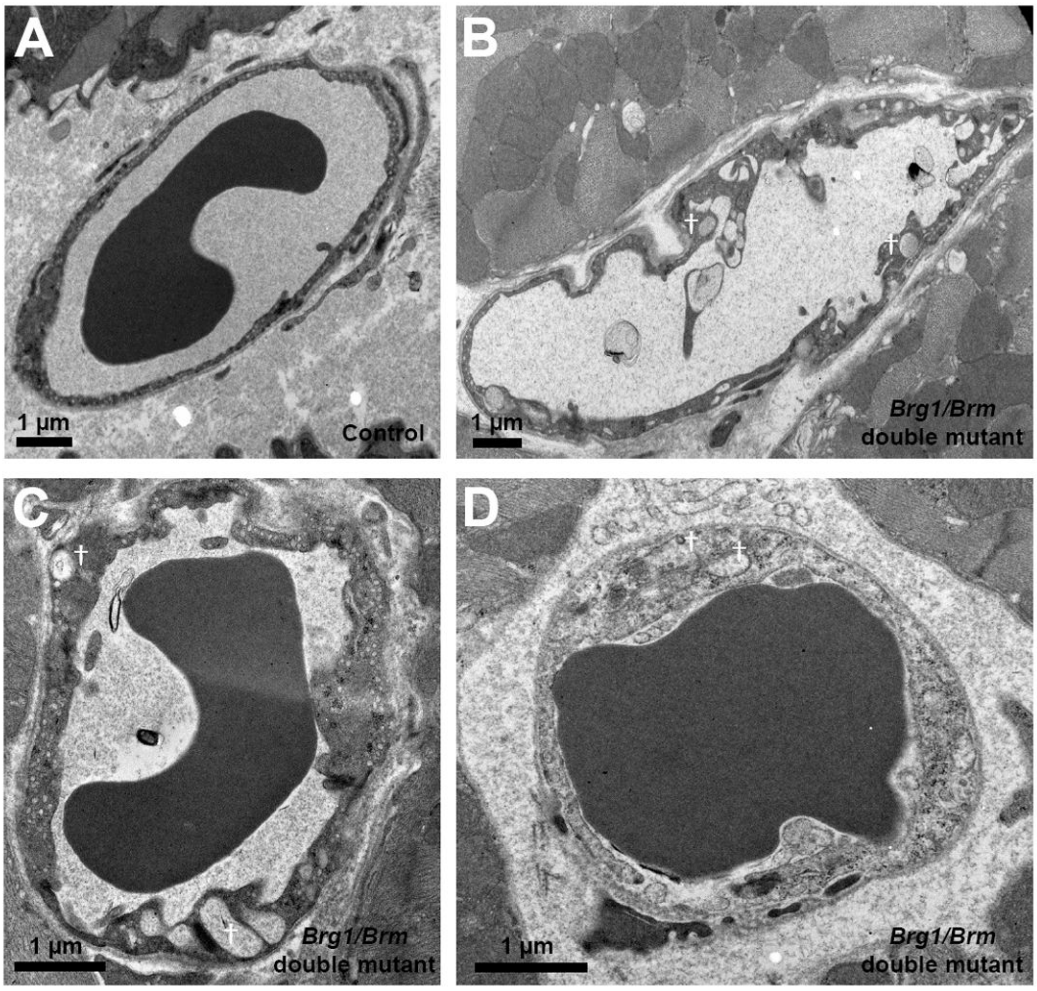

Figure 6. Changes in VECs occur as early as 14 days after the first pI-pC treatment of *Brg1/Brm* double-mutant mice

TEM analysis of cardiac endothelial cells demonstrates the vesicular changes and the non-uniform increase in VEC thickness in *Brg1/Brm* double-mutant mice 14 days after the first pI-pC treatment **(B-D)**, which are pronounced compared to control mice **(A)**. Dying endothelial cells were not found in cardiac VECs as they were at day 25. Examples of vesicles of increased size (†) are found in most capillary sections. Data are from animals 2516 (A) and 2520 (B-D). All panels correspond to the epicardium.

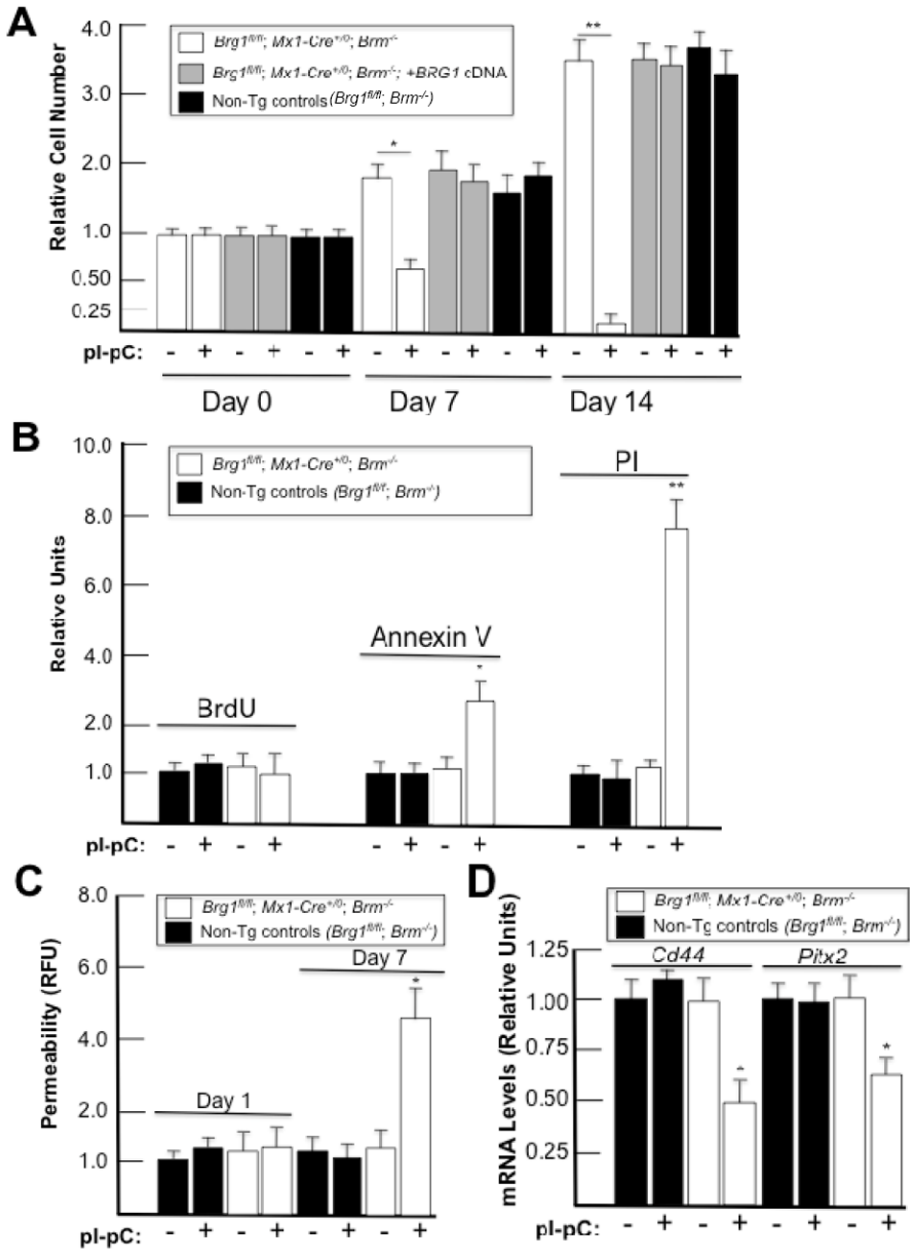

Figure 7. BRG1/BRM are required for VEC survival

A, Numbers of primary VECs from *ex vivo* cultures on days 7 and 14 relative to the first pI-pC treatment (day 0). **B,** Levels of BrdU incorporation (left), annexin V (center), and propidium iodide (PI, right) in VECs 7 days after first pI-pC treatment. Values are normalized to μg DNA and presented relative to untreated non-Tg controls for each assay. **C,** Permeability of VECs 1 and 7 days after the first pI-pC treatment relative to untreated non-Tg controls. **D,** RT-qPCR analysis of *Cd44* and *Pitx2* mRNA levels normalized to *Gapdh* levels in VECs at day 7. For each panel, the results are presented as mean ± SE from 3 independent experiments with significant differences indicated (*p<0.01; **p<0.001).

Table 1

Echocardiographic analysis of *Brg1/Brm* double-mutant mice at baseline and 1 day pre-mortem compared to parallel treated non-Tg and and untreated Tg littermates

Baseline values acquired one day after the final pI-pC treatment; 1-day pre-mortem values were acquired one day before the death of each treated double mutant; final values of controls acquired at the end of the experiment (1- day pre-mortem of longest surviving treated double mutant); all values are mean ± SE with significant differences indicated based on a one-way ANOVA followed by a Holm-Sidak pairwise comparison.

	Baseline UntreatedTg Controls (N=3)	Final Untreated Tg Controls (N=3)	Baseline Treated Non-Tg Controls (N=3)	Final Treated Non-Tg Controls (N=3)	Baseline Treated Double Mutants (N=9)	1 Day Pre-Mortem Treated Double Mutants (N=9)
Body Weight (g)	19.9+1.2	25.5+1.1‡	20.4+1.7	25.1+1.2‡	18.1+0.6	17.8+0.6†
HR (bpm)	739+5	747+8	689+17	757+19	625+41	438+59**
IVS;d	0.96+0.01	1.06+0.02	0.94+0.02	1.04+0.01	1.04+0.04	1.84+0.11*
LVID;d	2.52+0.10	3.0+0.19	2.71+0.16	2.94+0.16	2.45+0.07	2.16+0.13**
LVPW;d	0.99+0.02	0.98+0.03	0.91+0.02	0.98+0.02	1.02+0.04	1.56+0.11*
IVS;s	1.55+0.03	1.76+0.08	1.50+0.05	1.73+0.04	1.70+0.05	2.4+0.1*
LVID;s	1.13+0.08	1.27+0.10	1.19+0.08	1.34+0.10	1.03+0.04	0.94+0.10***
LVPW;s	1.39+0.01	1.45+0.03	1.47+0.07	1.57+0.07	1.56+0.05	1.98+0.13**
LV Vol;d	23.0+2.1	35.4+5.2	27.7+3.8	33.7+4.2	21.8+1.6	16.3+2.7†
LV Vol;s	3.0+0.5	4.1+0.8	3.4+0.5	4.6+0.9	2.3+0.3	2.1+0.36†
EF%	87.3+1.1	88.6+0.5	87.7+0.4	86.2+0.9	89.3+0.8	87.8+2.4
FS%	55.1+1.4	57.4+0.6	56.0+0.4	54.3+1.0	58.0+1.2	56.8+3.0
LV Mass	77.1+5.1	106.9+10.1	79.5+8.1	102.2+6.7	82.9+6.3	173.5+15.9**
LV Mass/BW	3.88+0.18	4.01+0.02	3.83+0.09	4.3+0.2	4.6+0.5	9.92+0.64*

*p<0.001 vs. all other groups;

**p<0.05 vs. all other groups;

***p<0.05 vs. final untreated Tg, final treated non-Tg controls, and baseline treated double mutants;

†p<0.05 vs. final untreated Tg, final treated non-Tg controls

‡p<0.01 vs. baseline

Abbreviations: BW, body weight; LV, left ventricle; HR, heart rate; LVEDD, LV end diastolic dimension; LVESD, LV end systolic dimension; LV EF%=[(LV Vol;d-LV Vol;s/LV Vol;d)*100]; LV Vol; d, LV volume in diastole; LV Vol;s, LV volume in systole.